

Article

Effects of Climate Change on Hydrology in the Most Relevant Mining Basin in the Eastern Legal Amazon

Paulo Rogenes M. Pontes , Rosane B. L. Cavalcante , Tereza C. Giannini , Cláudia P. W. Costa, Renata G. Tedeschi, Adayana M. Q. Melo  and Ana Carolina Freitas Xavier 

Vale Institute of Technology—Sustainable Development (ITV-DS), Belém 66055-090, PA, Brazil; rosanecavalcante@gmail.com (R.B.L.C.); tereza.giannini@itv.org (T.C.G.); claudia.costa@itv.org (C.P.W.C.); renata.tedeschi@itv.org (R.G.T.); adaymelo75@gmail.com (A.M.Q.M.); anacarolinaf.xavier@gmail.com (A.C.F.X.)
* Correspondence: p.rogenes@gmail.com

Abstract: The Itacaiúnas River basin, an important watershed for the mining sector in Brazil, has had 51% of its native forest area deforested in the last forty years. It is in the arc of deforestation of the Amazon. It has protected areas essential to local biodiversity maintenance, in addition to owning ore reserves. Here, we present the first study to assess the mean annual, seasonal, and spatialized hydrological processes, providing results on a detailed scale in the basin, including mining sites. We used five future projections of mean monthly temperature and daily precipitation as input to the MGB hydrological model to simulate how hydrological processes, such as evapotranspiration, water availability, and high flows, may change in the next 30 years. The future decrease in precipitation (−8%) and increase in temperature (10%) may strengthen the monsoon seasonal cycle and lengthen the dry month for evapotranspiration. Furthermore, some parts of the basin expect an increase in the high flows (8.1%) and a decrease in water availability (−93.6%). These results provide subsidies to develop adaptation strategies to ensure the viability of mining operations and safeguard the surrounding environment and communities.

Keywords: climate change; hydrological processes; MGB hydrologic model; Itacaiúnas River



Citation: Pontes, P.R.M.; Cavalcante, R.B.L.; Giannini, T.C.; Costa, C.P.W.; Tedeschi, R.G.; Melo, A.M.Q.; Xavier, A.C.F. Effects of Climate Change on Hydrology in the Most Relevant Mining Basin in the Eastern Legal Amazon. *Water* **2022**, *14*, 1416. <https://doi.org/10.3390/w14091416>

Academic Editor: Young Gu Her

Received: 16 March 2022

Accepted: 25 April 2022

Published: 28 April 2022

Publisher's Note: MDPI stays neutral with regard to jurisdictional claims in published maps and institutional affiliations.



Copyright: © 2022 by the authors. Licensee MDPI, Basel, Switzerland. This article is an open access article distributed under the terms and conditions of the Creative Commons Attribution (CC BY) license (<https://creativecommons.org/licenses/by/4.0/>).

1. Introduction

Identifying and characterizing the impacts and vulnerabilities of climate change in particular locations and industries are important for allowing stakeholders and regulators to take proactive approaches to moderate risk [1,2]. For activities where the alternative of moving is not an option, it is even more important. The mining sector, tied to geology, is a significant contributor to the development of many countries worldwide, but is particularly vulnerable to climate change. Therefore, climate changes risks should be considered in the long-term adaptation strategy of the industry.

In Brazil, the mining industry represents about 5% of the GDP, reaching 10% if indirect influence is also considered [3]. In 2020, iron, copper, manganese, and nickel ore constituted 13.6% of exports (Observatory of Economic Complexity-OEC). On the other hand, the mining sector is an extractive industry, and it is responsible for environmental (e.g., water resources use and land-use changes) and social impacts (e.g., conflict with indigenous people). In order to maximize the positive and minimize negative externalities, the mining industry is continually updating its practices regarding sustainability [4–8].

Climate change can alter air temperature and precipitation in different ways [9–13]. Depending on the region, it may lead to serious problems related to increasing extreme flows [14], fire occurrences [15], tree mortality [16], evapotranspiration [17]; and decrease in water availability [18–21] and other ecosystems services [22–25].

For the Amazon region, future climate projections agree with the increase in air temperature [26]. Meanwhile, precipitation is projected to decrease in some regions of the

Amazon (approximately –30% in the Xingu, Tapajós, Negro, and downstream Amazon basins) and increase in others (35% in the upstream Amazon basin) [27,28]. These changes may also increase forest fires, impacting land cover and local biodiversity [29]. Although future scenarios have been considered, some studies indicate that climate change may have already impacted the frequency and intensity of extreme hydrological events, causing socioeconomic impacts [30–36]. A recent review surveyed 35 papers related to climate change effects on agriculture, environmental conservation, water availability, flood risk, groundwater, and hydroelectrical power generation in the Tocantins-Araguaia and Amazon River basins, which encompass the Brazilian Amazon biome [37].

Understanding its responsibility beyond mining sites and expanding its influence on the entire watershed, the mining industry is following the principles of the International Council on Mining and Metals—ICMM—that suggests a catchment-based approach for its projects and the improvement of the relationship between the different stakeholders in the basin. This is similar to what has occurred in the Itacaiúnas River basin (IRB), a sub-basin of the Tocantins River located in the Amazon biome in the state of Pará. In this state, for instance, is the most prominent iron mine in the world, and the land area (hectares) is devoted to mining activities is as follows: 6,563,874 (exploration activities), 206,823 (concessions), 22,269 (licensing), and 184,148 (artisanal mining) [38].

The IRB is a unique basin located in the arc-of deforestation of the Amazon, where 51% of its native forest area was deforested in the last forty years, and 12,000 km² of its area corresponds to national protected areas called Mosaic of Carajás, which is mostly covered by primary forest and presents important mineral reserves for exploration and is monitored and protected by a partnership between the Chico Mendes Biodiversity Conservation Institute (ICMBIO) and Vale S.A. [39]. In contrast to the Amazon region, there is a lack of research estimating the impacts of climate change on the local hydrology (e.g., high and low flows and evapotranspiration) for the IRB and its mining sites.

Therefore, this study aimed to understand how climate change would affect hydrological processes and water resource availability (actual evapotranspiration and discharge patterns) in the IRB, including a local assessment of possible impacts on mining activities. We used the MGB hydrological model to simulate changes in hydrological processes by comparing the results from the future climate projections (data from 2021 to 2050, available from 5 General Circulation models-GCMs) and with the reference period climate.

2. Study Area

The Itacaiúnas River (i.e., the IRB) (Figure 1) is a tributary of the Tocantins River located in the Eastern Amazon in Pará state. The IRB has a drainage area of approximately 41,500 km², of which 48% are deforested areas. Approximately one-quarter of the IRB corresponds to a mosaic of national conservation units and indigenous lands [40], commonly called the “Mosaic of Carajás” (MoC). Together, the eleven municipalities of IRB have approximately 700,000 inhabitants and have a gross domestic product (GDP) of approximately 7 billion USD (6% of the GDP of states of the Amazon biome <http://www.ibge.gov.br>, (accessed on 1 January 2021)). This area is home to the industrial extraction of iron ore, manganese, copper, and nickel, including the world’s largest iron ore mine. The export of the mining industry from the basin’s municipalities represents 74% of total exports of the state of Pará, although the basin occupies only 3% of the state’s area.

The basin has a monsoon climate [41]. The mean annual precipitation is 1900 mm, and 95% of this total occurs during the wet season (November to May). The mean discharge in the outflow of the IRB is approximately 900 m³/s [39]. In the last 40 years, the increase in temperature has caused an increasing trend in potential evapotranspiration, while no trend was observed for precipitation [42]. Additionally, intense deforestation in the region induced an increase in the mean, maximum and minimum streamflow values [39,42].

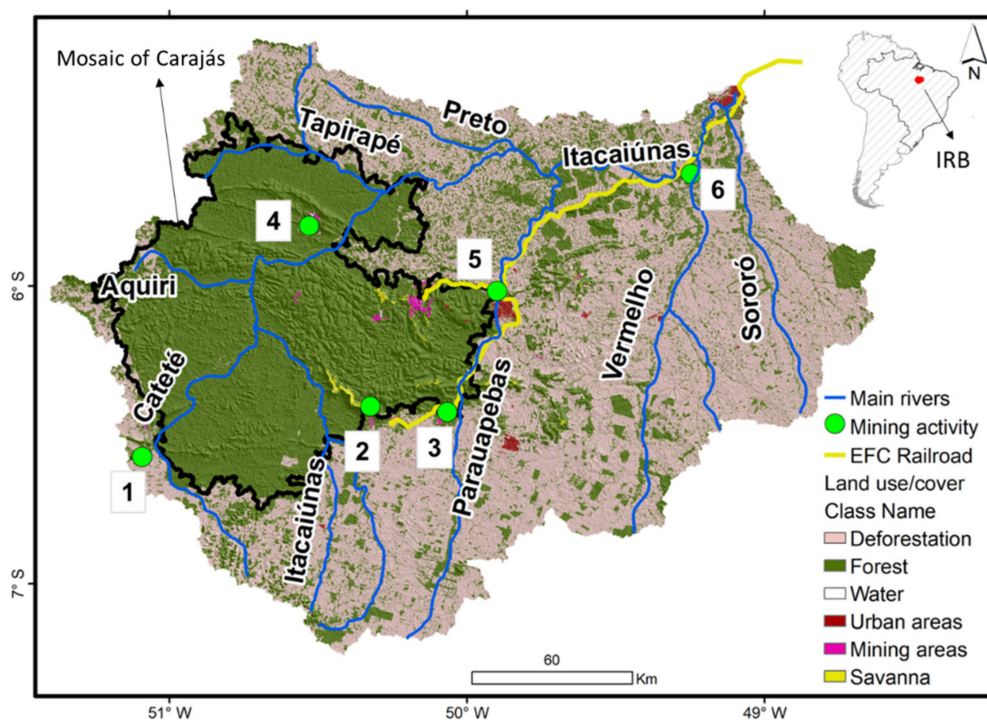


Figure 1. Itacaiúnas River basin location; the Mosaic of Carajás location; land-use classes; mining sites (Table 1) and main rivers.

Table 1. Description of the strategic points indicated in Figure 1.

ID	Description
1	Mining site: Downstream Onça-Puma
2	Mining site: Downstream S11D
3	Mining site: Downstream Sossego
4	Mining site: Downstream Salobo
5	Mining influence: Confluence Gelado × Parauapebas rivers
6	Mining railroad: Vermelho river

3. Materials and Methods

The methodological framework was divided into three steps (Figure 2): (i) data acquisition of the five GCMs; (ii) simulation of climate change scenarios with the hydrological model; and (iii) assessment of climate change impacts on hydrological processes.

3.1. Data Acquisition of GCMs

This study focused on assessing the impacts of climate change on hydrological processes (actual evapotranspiration and discharge) in two contrasting periods: the future period (2021–2050) and the reference period (1971–2001). All data have $0.5^\circ \times 0.5^\circ$ of spatial resolution. For the reference period, daily precipitation data were retrieved from the Water and Global Change Forcing Data (WFD) product and mean monthly air temperature data were retrieved from the Climatic Research Unit (<https://ir1.uea.ac.uk/cru/data>, accessed on 1 November 2020).

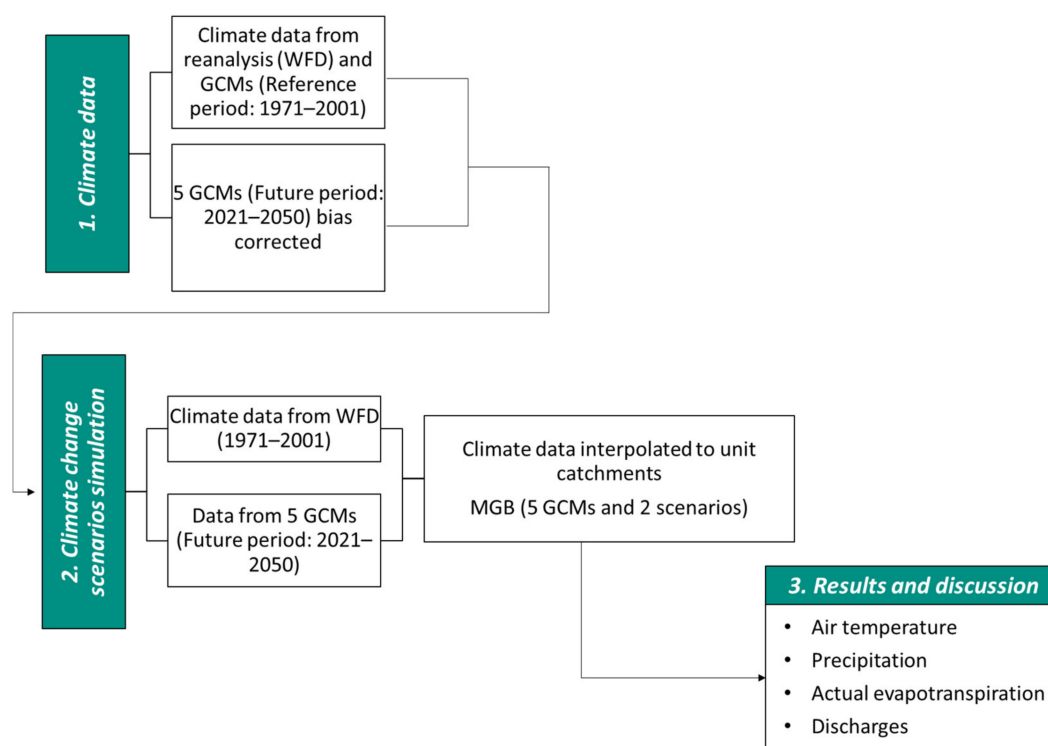


Figure 2. Methodological framework for assessing climate change impacts on the hydrological processes (AET: actual evapotranspiration; Q: discharge).

Five bias-corrected GCMs from the Coupled Model Intercomparison Project Phase 5—CMIP5 [43], bias corrected using WFD data [44] and available in the Earth System Grid Federation website (<https://esgf-index1.ceda.ac.uk/>, accessed on 1 November 2020), were used to provide future projections of mean monthly temperature and daily precipitation for two RCP scenarios (RCP4.5 and RCP8.5): GFDL-ESM2 M, HADGEM2ES, IPSL-CM5A-LR, MIROC-ESM-CHEM, and NorESM1 m (Table 2).

Table 2. GCMs and other information used in this study.

GCM	Spatial Resolution (Available in Earth System Grid Federation)	Institute	Country
GFDL-ESM2 M	0.5° × 0.5°	NOAA GFDL	United States
HADGEM2ES	0.5° × 0.5°	UK Met Office	United Kingdom
IPSL-CM5A-LR	0.5° × 0.5°	IPSL	France
MIROC-ESM-CHEM	0.5° × 0.5°	MIROC	Japan
NorESM1-M	0.5° × 0.5°	NorESM	Norway

The bias correction methods are often applied to future climate data to correct systematic deviations from observed data. The authors in [44] remove the bias between GCM and WFD using the trend-preserving statistical bias correction method based on quantile-mapping functions. The method follows two steps: (i) adjusts the long-term monthly mean of temperature (K) and precipitation (mm/day); (ii) adjusts the daily variability of temperature and precipitation, which, crucially, is a better representation of extreme events. The authors in [44] show that, in general, the GCM bias-corrected (long-term monthly and daily data) is better than the GCM uncorrected for the entire globe from 1960 to 2000 (reference period), including South America. In Brazil, for instance, the anomalies

(simulation-observation) of long-term monthly and daily temperature and precipitation bias-corrected reach values next to zero, showing the success of bias-correction techniques in representing the observed data.

3.2. Simulation of Climate Change with the Hydrological Model

3.2.1. The MGB Large-Scale Hydrological Model

The MGB (“Modelo de Grandes Bacias” in Portuguese; an acronym meaning “Model of Large Basins”) large-scale hydrological model [45,46] was used to simulate the changes in the hydrological processes due to the future climate projections compared to the reference period climate. The MGB is a semi-distributed rainfall-runoff model widely used mainly in South American river basins [47], although it has also been used in research on other continents, such as Africa [48].

The first step of MGB is to perform an algorithm to divide the entire watershed into small unit catchments. Physical features for each unit catchment are obtained from a digital elevation model (DEM) (river width and depth, river length, Manning coefficient, drainage area, and an estimate of the flooded area). Additionally, the percentage of land use/cover and soil type (hydrological response units-HRUs) for each unit catchment was calculated. Furthermore, the unit catchments can be grouped to represent macro-regions that have the same model parameter values.

The MGB has two modules that simulate hydrological processes. The vertical module simulates the water-energy balance and water bucket in each HRU, resulting in surface, subsurface, and groundwater streamflow values. These variables are routed to the rivers using a linear reservoir scheme [45]. Then, the discharge in each unit catchment is routed downstream in the horizontal module.

The Penman–Monteith equation [49] calculates evapotranspiration from the canopy (evaporation) and soil (directly or plant transpiration). The potential evapotranspiration, which considers the surface resistance equal to zero, is used to evaporate the precipitation intercepted in the canopy. The maximum canopy capacity is a function of the leaf area index. Soil evapotranspiration considers the variation in surface resistance as a function of soil moisture [45]. Surface resistance decreases as the soil moisture decreases from field capacity to wilting point. Finally, the actual evapotranspiration is the sum of the canopy evaporation and soil evapotranspiration. Runoff is calculated based on the variable contribution area concept of the ARNO model [50]. Groundwater and subsurface are calculated using nonlinear and linear functions based on water availability in the soil [45].

3.2.2. The MGB Model Setup

Here, we used the same model setup presented in [39]. A 30 m DEM Alos World 3D [51] was used to divide the IRB into 1246 unit-catchments. A main channel rectangular cross-section was obtained from in situ information for each river reach: $w = 3 \times (0.91 \times A^{0.476})$, where “ w ” is the river reach width (m); “ A ” is the drainage area (m^2); and $d = 0.547 \times w^{1.146}$, where “ d ” is the full depth of the river reach (m). Manning’s coefficient was defined as 0.025 ($m^{-1/3} \cdot s$) for all river reaches. Additionally, we used the Shuttle Radar Topography Mission (SRTM) Bare Earth Data [52] and HAND model [53] to estimate the stage–area–volume curve for each unit-catchment [46,54].

The soil type map was obtained from The Digital Soil Map of the World (<http://www.fao.org/geonetwork>, accessed on 1 February 2022; at 1:5,000,000 scale). The land use/cover for 2018 was obtained from Landsat imagery [40], and the classification of these images generated five land use/cover types: forest, deforested land, urban, mine, savanna, and water areas. Combining the soil type and land use/cover maps, we obtained the HRUs. We considered the same land use/cover map for reference and future periods. Vegetation data (vegetation height, leaf index area, albedo, and superficial resistance) were obtained in [39]. For each HRU of a unit catchment, the soil parameters were defined and used to calibrate the MGB model. These parameters were set globally for all unit catchments. The results of the calibration and validation are presented in [39], and the model performance results

were considered satisfactory. The Nash–Sutcliffe efficiency, Nash–Sutcliffe logarithmic discharges, and long-term relative error values were 0.66, 0.70, and 17%, respectively, for the first period assessed (1987 to 1989, when the land cover was mainly native forest) and 0.39, 0.70, and 21%, respectively, for the second period (1998 to 2007, when pasture areas replaced 30,000 km² of the native forest).

The precipitation and air temperature from the WFD product were used to simulate the reference period. To simulate the future period (both RCP4.5 and RCP8.5 scenarios), we used the precipitation and air temperature from the five bias corrected GCMs. Other climate data used as inputs of MGB (wind speed, solar radiation, relative humidity, and air pressure, all data in the surface) were obtained from the Climate Research Unit (CRU) with a 10' spatial resolution and long-term averages, and we considered the same information for the reference and future periods. All climate data were interpolated for each unit catchment using inverse distance weighting.

3.2.3. Assessment of Climate Change Impacts on Hydrological Processes

To evaluate the impact of climate change on hydrological processes in the IRB, we applied the MGB model to the reference period and the two climate scenarios. We compared the mean annual and monthly precipitation (P), temperature (Temp), actual evapotranspiration (AET), and discharge (Q) in the IRB for the reference period and the GCMs (individually and the mean of the GCMs) for both RCP scenarios. A two-sample *t*-test (at the 5% significance level) was used to evaluate the statistical significance of the future changes in these variables. For the discharge, we also compared the monthly values of the coefficient of variation and the exceedance probability curve of daily discharge to analyze the occurrence of extreme flows.

We also carried out a spatial assessment of the mean annual values of these P, Temp, and AET, and of the discharges with an exceedance probability of 90% (Q90, a low reference discharge) and 5% (Q5, a high reference discharge), focusing on analyzing the changes in the protected areas (Mosaic of Carajás) and at strategic points for mining activity in the basin (Table 1 and Figure 1).

4. Results

4.1. Air Temperature and Precipitation

Table 3 presents the mean annual precipitation and temperature in the reference period (WFD and CRU) and future period (each GCM individually and the mean of the 5 GCMs), and the mean relative difference (MRD) between the mean of GCMs (mGCMs) and WFD. All the GCMs agreed with an increase in mean air temperature and a decrease in mean annual precipitation in the IRB in the future period (2021–2050) but with different intensities. A higher variation (coefficient of variation of 5.5%) between the GCMs was observed for the projection of the annual precipitation for RCP8.5. The mGCMs indicated an increase of 2.2 °C in the air temperature of the IRB (RCP4.5) and 2.7 °C (RCP8.5). The mean estimated decrease in annual precipitation was 121 mm for RCP 4.5 and 156 mm for RCP 8.5.

Although all GCMs indicated annual average precipitation lower than that of the reference period for both scenarios, the models indicated different levels of variability in the annual precipitation (Figure 3). The IPSL indicated the highest average annual precipitation caused by years with very high total annual precipitation, especially in the RCP4.5 scenario. The GFDL indicated a higher frequency of years with annual average precipitation less than the reference period.

Table 3. Mean annual precipitation and temperature in the reference period (WFD) and future period (each GCM and mGCMs), and the mean relative difference (MRD) between the GCMs’ mean and WFD.

Time Period	Data Source	Annual Precipitation (mm/Year)		Mean Annual Temperature (°C)	
		RCP4.5	RCP8.5	RCP4.5	RCP8.5
1971–2001	WFD	1937.8		25.9	
2021–2050	GFDL	1756.9	1635.4	27.8	28.1
	HADGEM2ES	1760.7	1745.4	28.5	28.8
	IPSL	1822.7	1928.0	28.2	28.5
	MIROC	1880.0	1758.7	28.2	29.2
	NORESM1 m	1861.5	1840.9	27.8	28.1
	Mean of GCMs	1816.4	1781.7	28.1	28.6
MRD between Mean GCMs and WFD		−6%	−8%	8%	10%

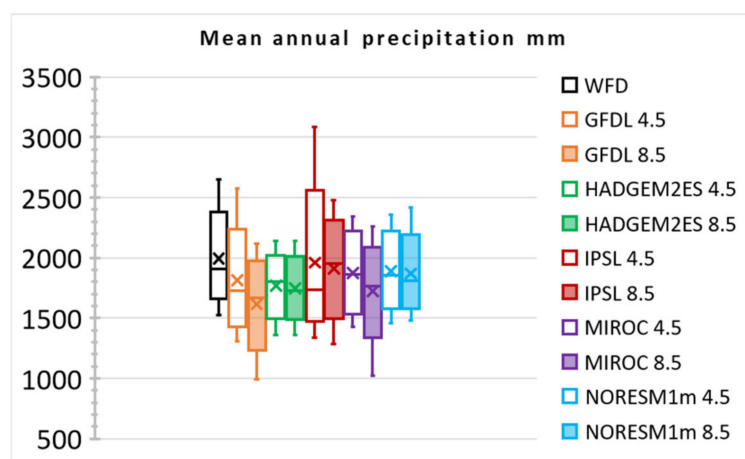


Figure 3. Boxplot of mean annual precipitation (mm/year) for each GCM and scenario (RCP4.5 and RCP8.5).

Figure 4 presents the monthly seasonality of precipitation in the IRB. All models indicated a decrease in the monthly mean precipitation from June to November in both scenarios. Considering the mGCMs, the future precipitation for these months will be 50% lower than the reference period. These six-month periods currently account for 25% of the annual precipitation but will decrease to 13% under RCP8.5. The number of months with mean precipitation lower than 100 mm can increase from four (June to September) to six (May to October). The rainiest trimester is January to March in the reference and future periods, except for the predicted precipitation with the MIROC model (which indicates that the rainiest trimester is from December to February). At least four GCMs indicated increasing precipitation during these months in the future, and the mGCMs indicated an increase of 9.6% in the precipitation of this trimester.

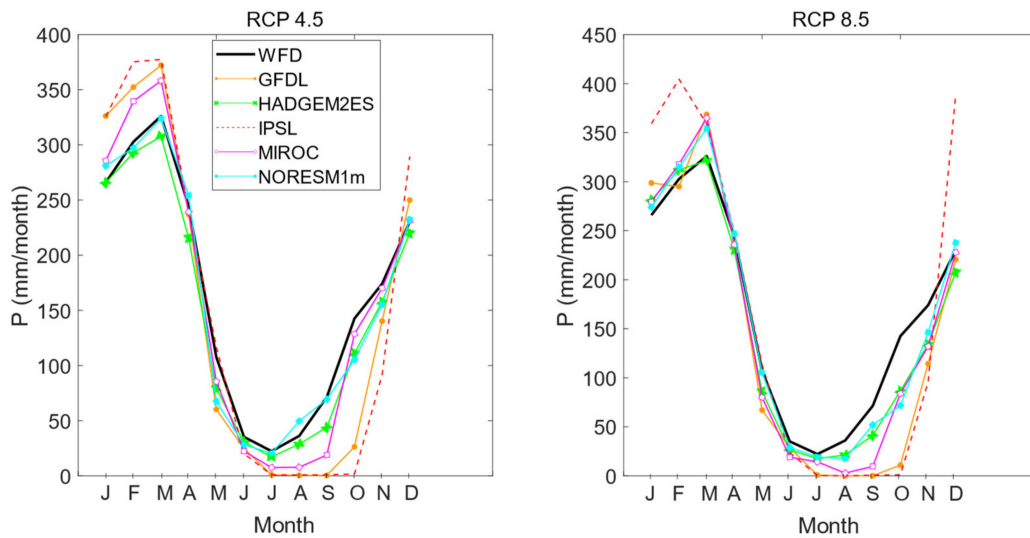


Figure 4. Mean monthly precipitation (mm/month) in the IRB for the WFD, each GCM, and both RCP scenarios.

Figure 5 presents the monthly seasonality of temperatures for present and future periods. All GCMs agree with the increase in mean monthly temperature. Similar to the present seasonality, the future period is characterized by two peaks of temperature (May and October), and the highest temperatures occur during dry months.

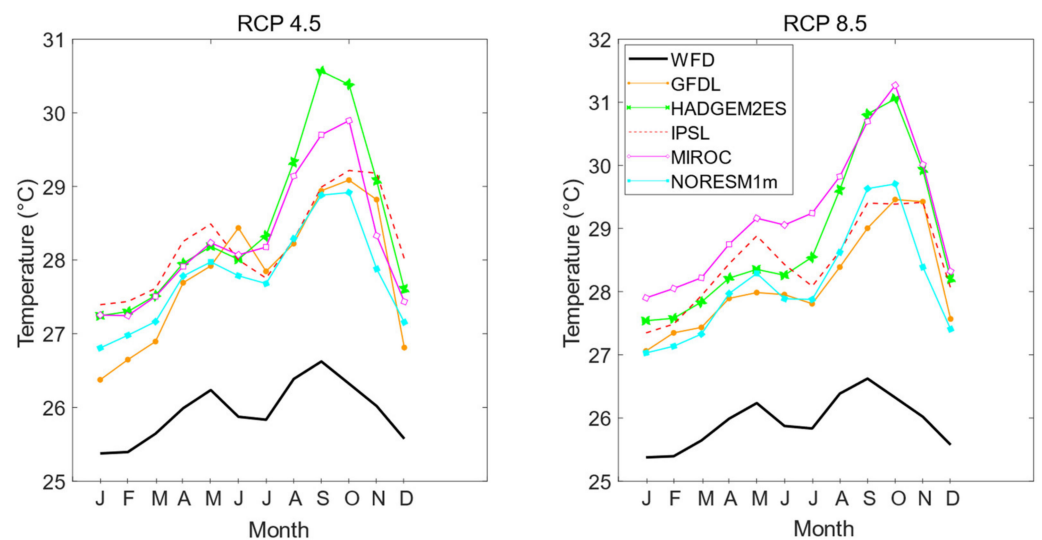


Figure 5. Mean monthly temperature (°C) in the IRB for the WFD, each GCM, and both RCP scenarios.

The spatialized assessment of mGCMs shows a decrease in the annual average precipitation for the future period compared to the reference period in all unit catchments of the IRB (Figure 6). The highest differences were observed in the southwestern part of the basin, where the average values of annual precipitation in the future period (RCP8.5) were up to 288 mm/year, decreasing in the north-east, where precipitation can reach 151 mm/year. The mean annual temperature (mGCMs) increases in all unit-catchments (Figure 7). The mean absolute differences between the temperature of mGCMs and reference periods increase from west to east of the IRB. The mining sites are mainly affected by a decrease in precipitation, which may cause a reduction in water availability. Furthermore, the increase in temperature in the west added to land cover may increase forest fires.

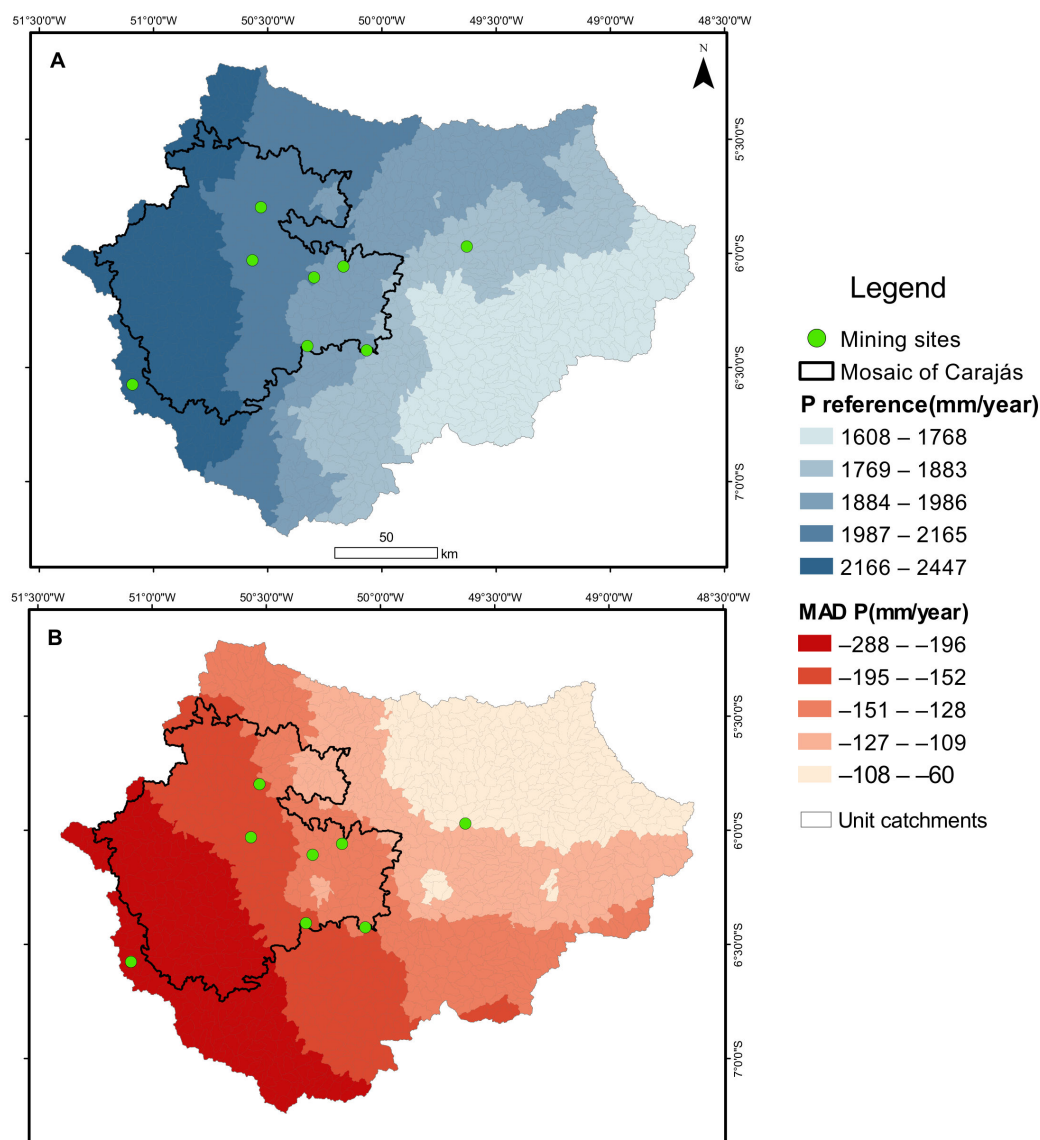


Figure 6. (A) Mean annual precipitation P (mm/year) for the reference period; and (B) mean absolute differences (mm/year) of mean annual precipitation between the future (mGCMs) and reference periods for the RCP8.5 scenario (we decided not to show the results of RCP4.5 because the results showed similar spatial patterns).

In the MoC, the mGCMs indicated that the mean annual temperature increased by 6% (RCP4.5) and 8% (RCP8.5) in comparison with the reference period, while out of MoC, these values were 9% (RCP4.5) and 11% (RCP8.5). Mean annual precipitation was the opposite. The mGCMs indicated a decrease of 7% (RCP4.5) and 9% (RCP8.5) in the MoC, and a decrease of 6% (RCP4.5) and 7% (RCP8.5) out of MoC.

t-test indicated significant changes in the mean annual precipitation of the GFDL and HADGEME2S (both RCP4.5 and RCP8.5) and MIROC (RCP8.5) in comparison with the WFD. The mean annual precipitation of all GCMs also indicated significant changes in the future. All GCM models and the mGCMs indicated significant changes in mean monthly precipitation, except in May, for both scenarios.

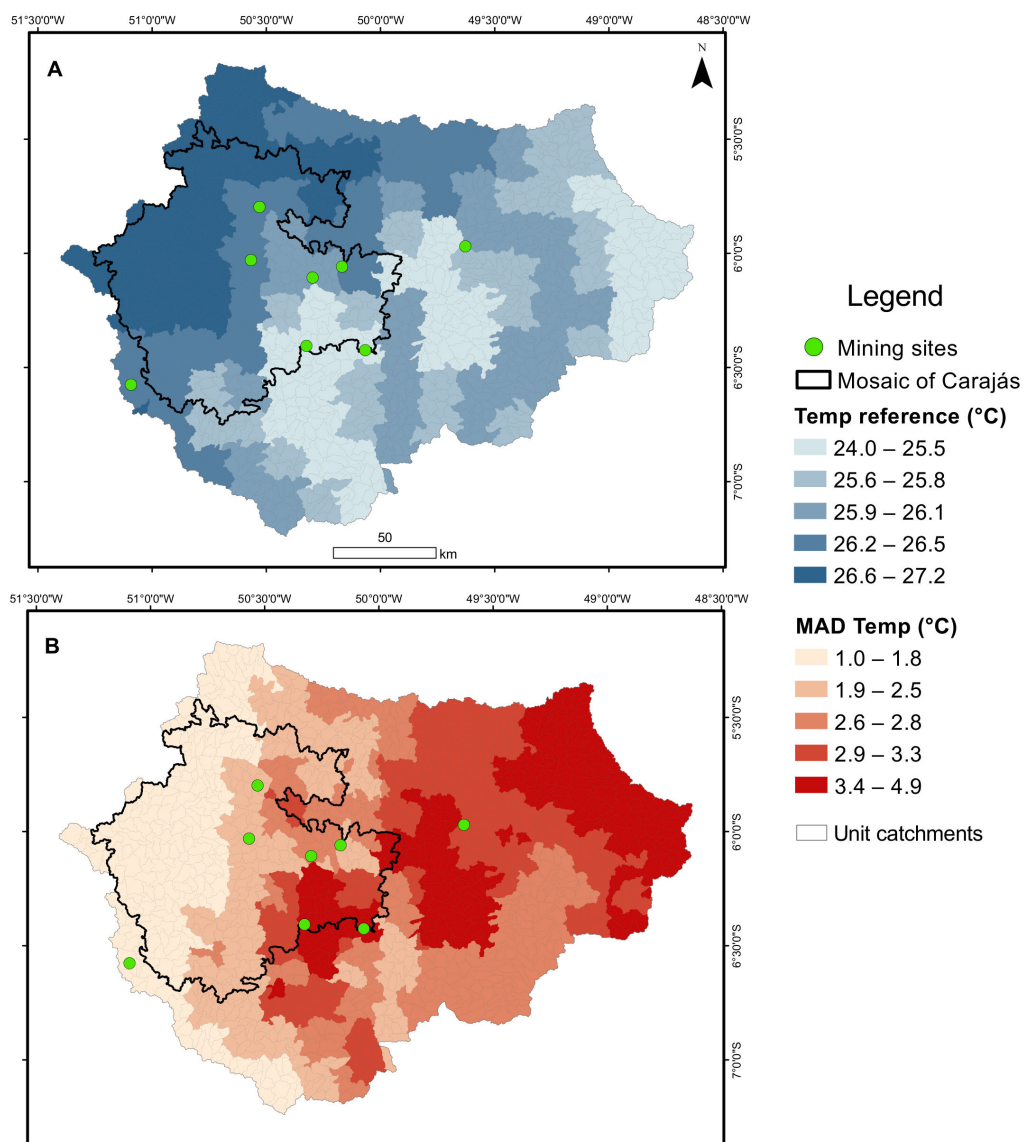


Figure 7. (A) Mean annual temperature Temp ($^{\circ}\text{C}$) for the reference period, and (B) mean absolute differences ($^{\circ}\text{C}$) of mean annual temperature between the future (mGCMs) and reference periods for the RCP8.5 scenario (we decided not to show the results of RCP4.5 because the results showed similar spatial patterns).

4.2. Evapotranspiration

The mean annual AET in the IRB in the reference period was 1218.4 mm/year, while the annual average AETs of the IRB for the five GCMs were 1126.3 mm/year and 1112.4 mm/year for RCP4.5 and RCP8.5, respectively (Table 4). Comparing the GCMs, the lowest AET was estimated from the GFDL and RCP8.5 scenario (influenced by a year with low precipitation), and the highest AET was estimated from HADGEM2ES and RCP4.5 (Figure 8).

Table 4. Mean annual actual evapotranspiration in the reference period (WFD) and future period (each GCM and mGCMs), and the mean relative difference (MRD) between the GCMs' mean and WFD.

Time Period	Data Source	Annual AET (mm/Year)	
		RCP4.5	RCP8.5
1971–2001	WFD	1218.4	
2021–2050	GFDL	1050.2	1025.4
	HADGEM2ES	1204.9	1190.6
	IPSL	1050.9	1068.9
	MIROC	1140.2	1115.2
	NORESM1 m	1185.6	1161.9
	Mean of GCMs	1126.3	1112.4
MRD between Mean GCMs and WFD		−8%	−9%

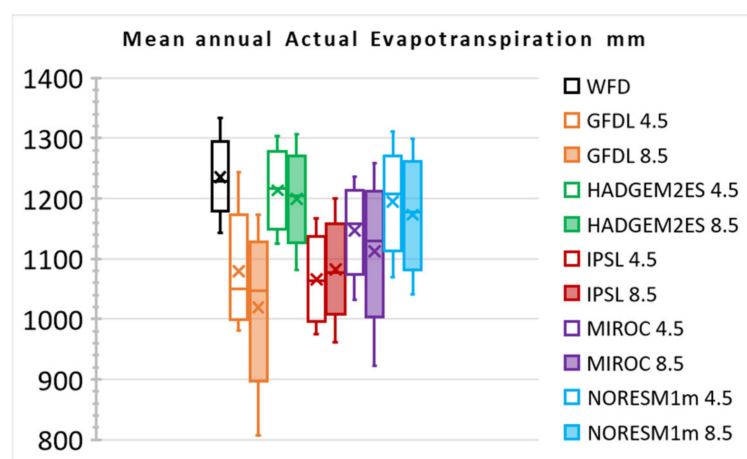


Figure 8. Mean annual evapotranspiration AET (mm/year) for each GCM and both scenarios in the IRB.

The AET did not exhibit seasonality for the reference period, which was probably due to a combination of higher canopy interception during the rainy season and evapotranspiration sustained by soil water storage during the dry season, as suggested by [55]. However, a strong decrease in AET from August to December is predicted in the future scenarios for all models, especially from September to November, using the data from IPSL and GFDL (Figure 9). The reduction in AET indicates that the terrestrial water storage will not sustain the higher potential evapotranspiration in the longest dry period predicted in future scenarios. The values of AET estimated by HADGEM2ES and NORESM1 m were similar to the AET estimated by WFD, mainly from January to May. They also predicted an increase in the mean AET at the beginning of the dry period (June and July).

The mGCMs indicated a decrease in actual evapotranspiration for the future period compared to the reference period in all unit catchments of the IRB (Figure 10). The spatial variation indicated that the changes in precipitation, rather than temperature, were the main factor responsible for the changes in actual evapotranspiration. The highest differences were observed in the southwestern part of the basin, but the differences decreased in the northeastern part of the river basin. At the mining sites, the relative changes between the future and reference periods indicated decreases of up to 200 mm and 160 mm in the mean annual actual evapotranspiration and streamflow under RCP8.5, respectively.

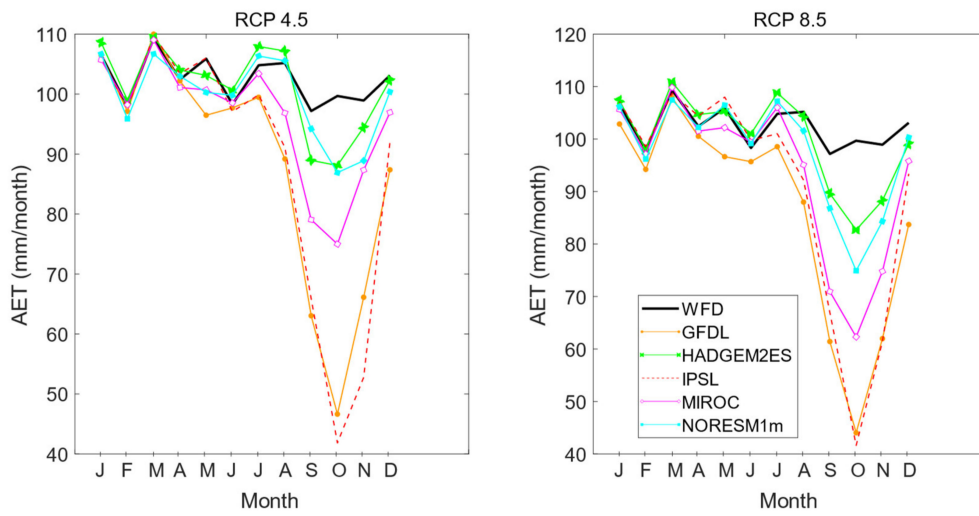


Figure 9. Seasonality of mean monthly AET (mm/month) in the IRB. The values are estimated for the reference and future periods for all GCM and the RCP4.5 and 8.5 scenarios.

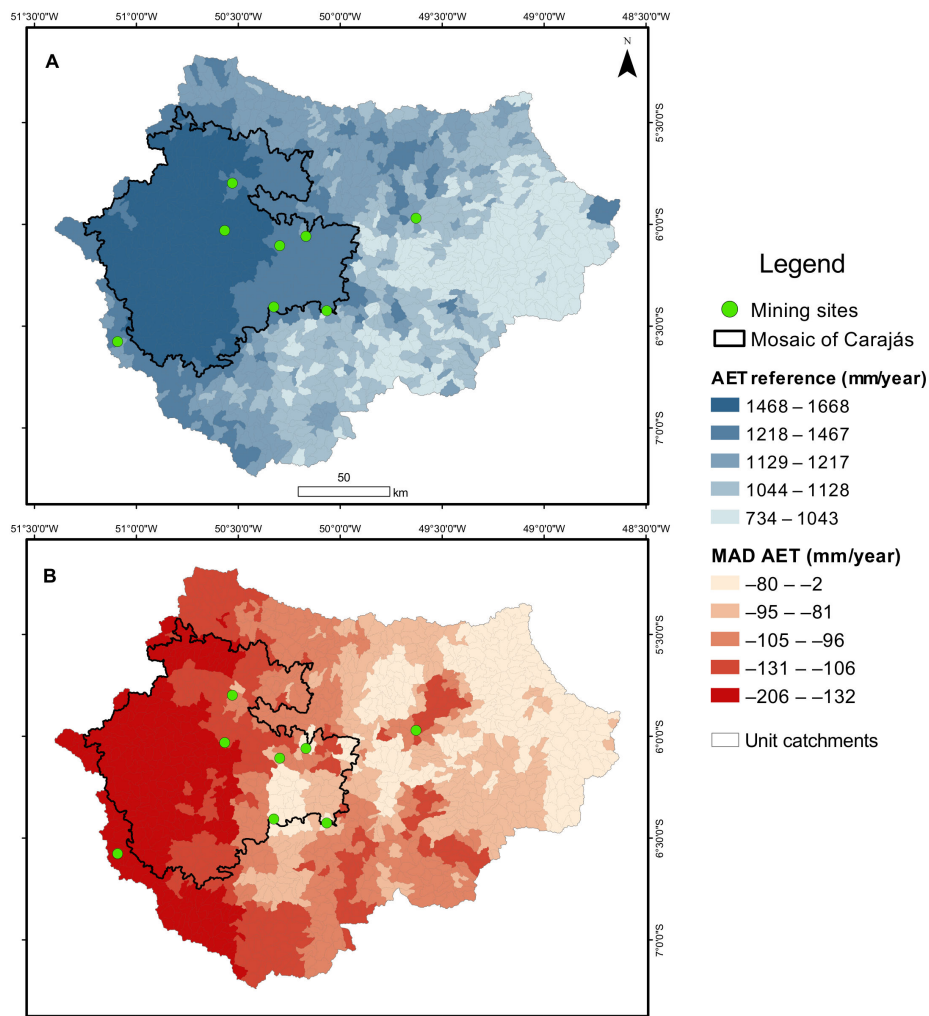


Figure 10. (A) Annual average actual evapotranspiration AET (mm/year) for the reference period; and (B) mean absolute differences (mm/year) of annual average AET between the future (mGCMs) and reference periods for the RCP8.5 scenario (we decided not to show the results of RCP4.5 because the results showed similar spatial patterns).

The Mosaic of Carajás is the region with the highest AET in the reference period (mean annual AET of 1500 mm/year versus 1100 mm/year outside of the mosaic). The mean annual AET in MOC was 1377 (RCP4.5) and 1362 mm (RCP8.5), as calculated by the mean of the GCMs. Outside of the Mosaic of Carajás, the mean annual AET in the future period was 1022 and 1009 mm in the RCP4.5 and RCP8.5 scenarios, respectively.

All the GCMs indicated significant changes in the mean annual AET, except for the AET estimated using input data from HADGEM2ES (only RCP4.5), including the mean annual AET of all models. Like precipitation, all GCM models and the mGCMs indicated significant changes in the mean monthly AET for both scenarios, except in May.

4.3. Discharges

For RCP4.5, while IPSL, MIROC, and GFDL models indicated an increase in the outlet discharges in the future compared with that in the reference period, HADGEM2ES and NORESM1 m indicated the opposite result (Figure 11 and Table 5). These models predicted a lower reduction in precipitation during the dry season and a higher AET, and these values were closer to those calculated for the reference period. For RCP8.5, only the discharges estimated using the input of IPSL (1203 m³/s) were greater than those for the reference period (946 m³/s).

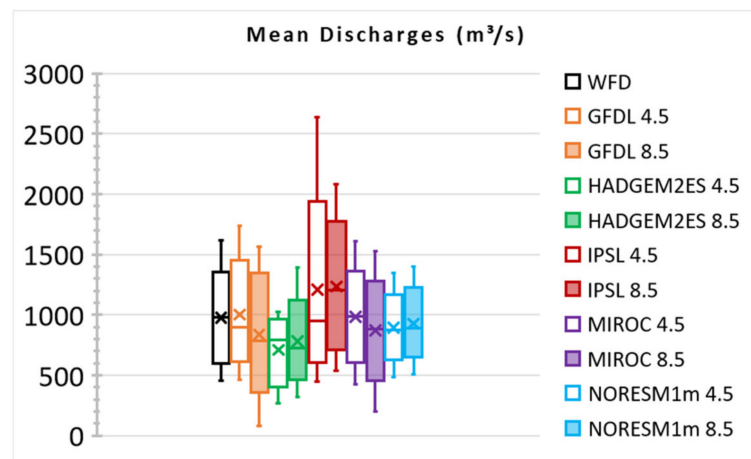


Figure 11. Mean discharges (m³/s) for each GCM and both scenarios in the IRB.

Table 5. Itacaiúnas River basin flow in the reference period (WFD) and future period (each GCM and mGCMs), and the mean relative difference (MRD) between the GCMs’ mean and WFD.

Time Period	Data Source	Discharge (m ³ /s)	
		RCP4.5	RCP8.5
1971–2001	WFD	946	
	GFDL	973	828
2021–2050	HADGEM2ES	723	748
	IPSL	1028	1203
	MIROC	975	867
	NORES M1 m	896	912
	Mean of GCMs	919	911
	MRD between Mean GCMs and WFD	–3%	–4%

Figure 12A,B present the seasonality of discharges in the IRB for the reference period and the future period for each GCM and RCP scenario. Regarding the mean monthly discharges estimated by the RCP4.5 scenario, at least 4 of the 5 GCMs indicated discharges

lower than the reference period from June to December due to the long dry period. The reduction in discharges calculated using the five GCMs in these months varied from 16 to 59% compared to the reference period. In general, the discharges obtained from all GCM input data indicated an increase relative to the reference period from January to May, except for the discharge obtained from HADGEM2ES. Regarding monthly discharges estimated by RCP8.5, all models indicated a reduction in discharges from June to December, which varied from 14 to 68%.

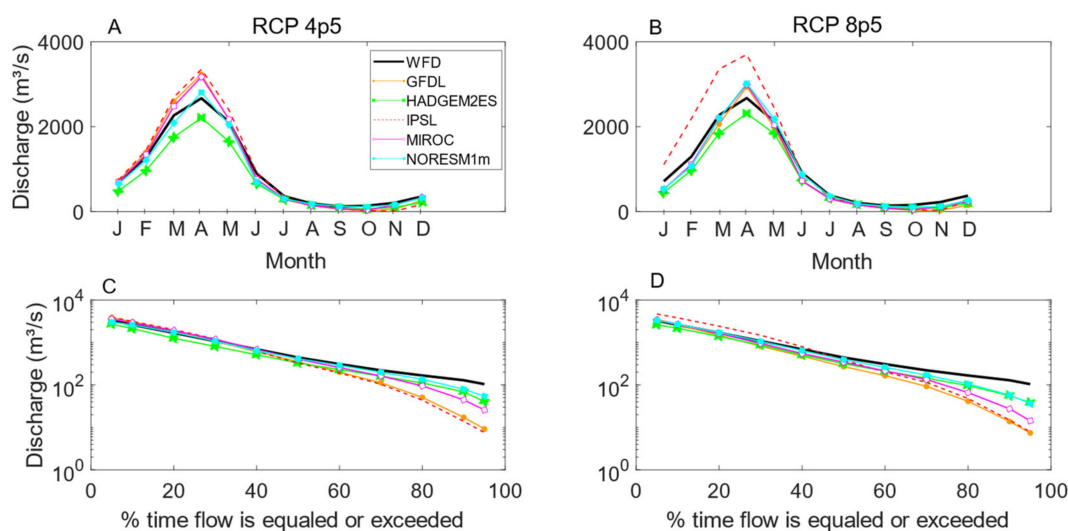


Figure 12. Seasonality of discharge (A,B) and exceedance probability of discharges (C,D) obtained using the input data for each GCM and both scenarios in the IRB. The black line presents the discharges obtained using the WFD input data.

Figure 12C,D present the flow duration curves using the input data for each GCM and both scenarios. All the future discharges with a 90% exceedance probability (Q_{90} , discharge exceeded or equaled in 90% of the time, Figure 12C,D) estimated by GCMs were lower than those of the reference period. The result implies less legal water availability for water users in the IRB. Mean Q_{90} of the GCM models indicated a reduction of $85 \text{ m}^3/\text{s}$ (RCP4.5) or $95 \text{ m}^3/\text{s}$ (RCP8.5) in the future compared to the reference period. Future mean Q_5 (discharge with a 5% of exceedance probability) indicated an increase of $150 \text{ m}^3/\text{s}$ (RCP4.5) or $210 \text{ m}^3/\text{s}$ (RCP8.5) in the future in comparison with the reference period. Despite the difference in discharges for the future and reference periods, the hypothesis test indicated significant changes only in the dry months for the mGCMs.

Figure 13 presents the monthly coefficient of variation (CV) in discharge for the reference and future periods. The results of the models indicated that the CV would decrease during the months with lower precipitation due to the predicted reduction in dry period precipitation. For RCP4.5, the GFDL and IPSL models presented higher CV values, surpassing 250% (GFDL) and 200% (IPSL) in November. For RCP8.5, the behavior of CV was similar to RCP4.5, but MIROC and NORESM1 m models presented higher CVs than that of the reference period.

The spatialized assessment of extreme flows shows a strong decrease in the Q_{90} , mainly in the western IRB. The reduction in Q_{90} could reach 100% in some rivers (unit-catchments), affecting all the mining sites (Figure 14A). Oppositely, the future projections indicate an increase in Q_5 , mainly in the eastern IRB, reaching 35%.

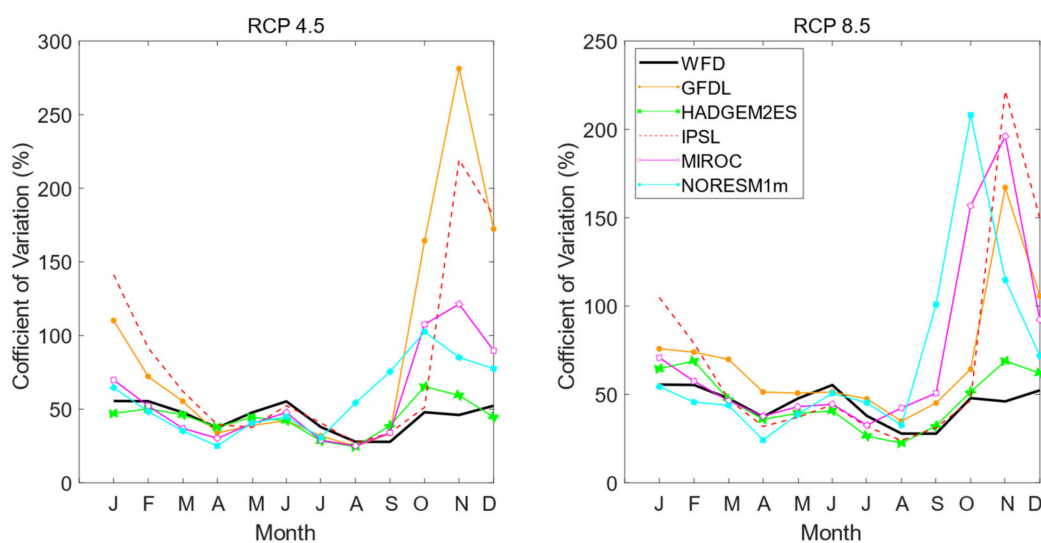


Figure 13. Monthly coefficient of variation in discharges for the WFD and GCM models and both scenarios.

Table 6 presents the MRDs for Q90 and Q5 discharges between the future and reference periods and both scenarios at the mining sites (Figure 1). Downstream of two mining sites (IDs 2 and 5), the Q90 is expected to be reduced by more than 90%. For the Q5 flow, the GCMs indicated an increase of up to 8.1% in the future period. The two sites with the highest estimates of increased maximum flows (Q5) already have flooding problems.

Table 6. Mean relative differences in Q90 and Q5 between the future and reference periods and both scenarios.

ID	Mean Relative Differences Q90 (%)		Mean Relative Differences Q5 (%)	
	RCP 4.5	RCP 8.5	RCP 4.5	RCP 8.5
1	−67.0	−75.4	0.8	1.3
2	−90.1	−96.7	0.2	2.3
3	−61.0	−69.4	3.2	3.4
4	−86.4	−93.6	2.6	5.3
5	−75.5	−85.1	4.7	8.1
6	−55.6	−63.8	3.8	6.6

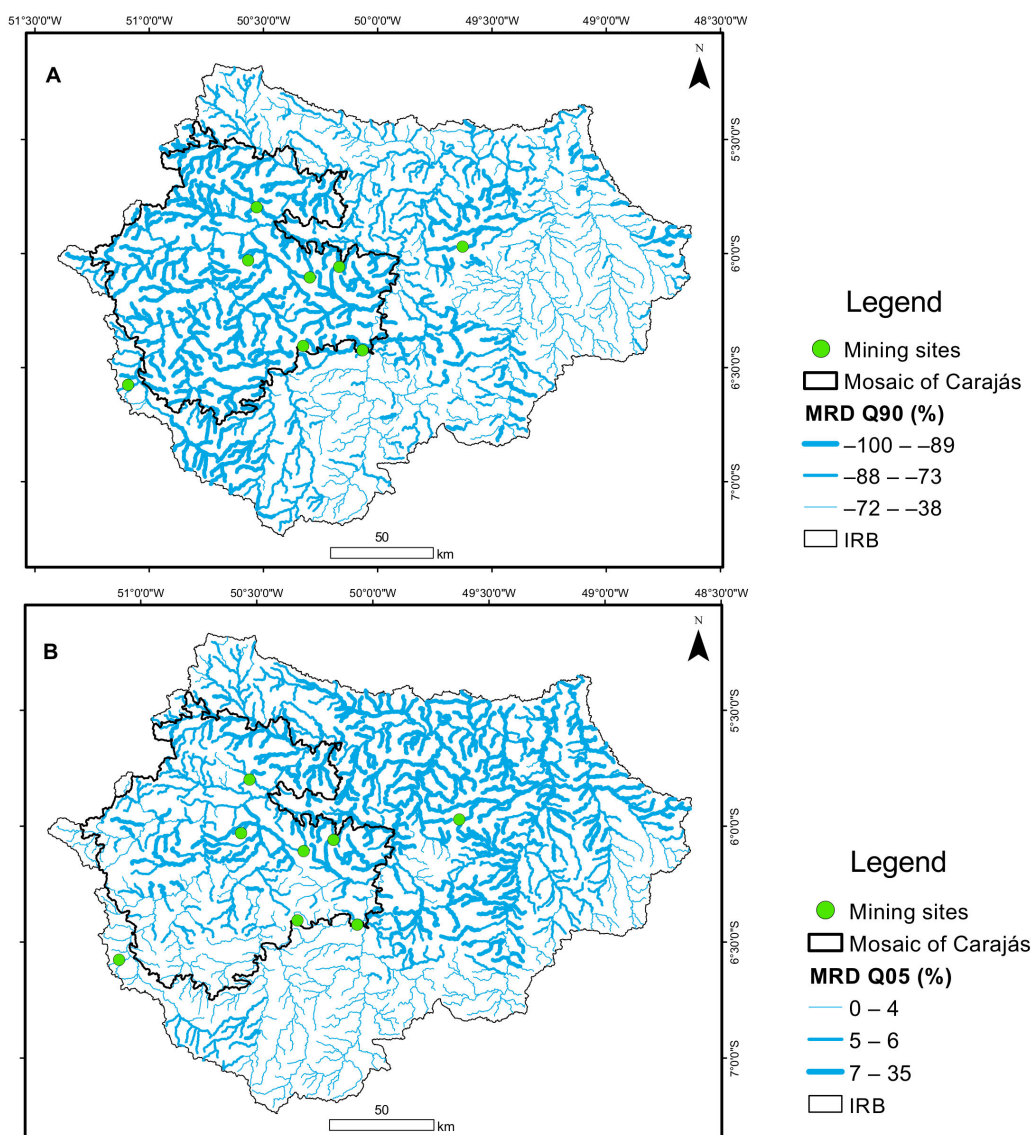


Figure 14. Mean relative differences in Q90 (A) and Q5 (B) between the future (RCP8.5) and reference periods and both scenarios spatialized in the IRB (we decided not to show the results of RCP4.5 because the results showed similar spatial patterns).

5. Discussion

5.1. Hydrological Modeling and General Circulation Model Aspects

We used air temperature (long-term mean monthly) and precipitation (daily) data to assess climate change. Precipitation is the primary input data in the regional hydrological cycle and it is strongly related to other meteorological variables in the equatorial climate zone (i.e., the Amazon region) [56].

As a simplification of this work, the relative humidity, sunshine duration, wind velocity, and atmospheric pressure were considered fixed for reference and future periods, which may be a limitation of this study, as sunshine duration and relative humidity influence the potential evapotranspiration estimates. In addition, the future climate estimated by the Sixth Assessment Report (AR6-IPCC) can modify the magnitude of changes in evapotranspiration and discharges simulated. The Manning coefficient was also considered fixed by river reach.

In the model simulations, the same land use and model setup were used for the reference and future periods to isolate the effect of the precipitation and temperature changes on streamflow. The change in forest land use for pasture since the 1970s generated

a significant increase in the flow in the basin during the period, with a slight opposite effect caused by climate variation [42]. The land use in the future simulations was considered constant and equal to the land use in 2018, which is unlikely to occur in the real world [57]. In addition to direct anthropogenic land-use changes, climate change can affect land cover. For example, the increase in temperature in the eastern region will make this region no longer suitable as a habitat for various pollinating and seed-dispersing forest species [58–60]. If deforestation continues in the basin, an increase in the streamflow is expected, as shown by [39]. This increase can enhance the increase in flow during the flood period but offset the changes in the monthly flow during the drought period.

Additionally, climate changes can promote changes in the type and characteristics of the vegetation. For example, a longer dry season is predicted, resulting in a very low AET for the end of the dry season, which can cause tree mortality and result in changes in the leaf index area, albedo, and superficial resistance.

The ensemble GCMs indicated a decrease in the mean annual precipitation of 8% (RCP8.5) or 6% (RCP4.5) and an increase in the mean air temperature of 10% (RCP8.5) or 8% (RCP4.5) compared to the reference period. This behavior is expected for ensemble GCMs in the eastern Amazon Basin [26,28,61]. Our results also indicate that the future could be drier (lower mean annual precipitation), following the results of [61] and [27] for the Amazon. However, the cited results may be related to dry biases of GCMs for the Amazon region, since the cited studies did not use bias-corrected data [27]. Using bias-corrected data, we found that all the five GCMs indicated a decrease in precipitation from June to November, with a mean value 50% lower than that in the reference period.

Ref. [62] assessed precipitation and air temperature anomalies from the future (ensemble of GCMs, 2070–2100) and present (CRU data, 1975–2005). The authors showed differences between the CGMs and CRU data for the southern Amazon. The values varied from +15% to –10% (wet season) and +10 to –60% (dry season) for the southern Amazon. Considering the ensemble of GCMs, our results indicated a decrease of 50% (dry season) and an increase of 9.6% (wet season) in future precipitation. The authors also indicated a decrease in evapotranspiration in the dry season in the southern Amazon, but this decrease was slighter than the reduction estimated in the current study. The water cycle (estimated by precipitation minus evapotranspiration) estimated by [62] indicated an austral summer in the future (2070–2100) that is wetter than that in the present period (1975–2005) in the southern Amazon. Our results indicate the opposite, except for the streamflow estimated using HADGEM2ES data.

Quantifying the uncertainties of temperature and precipitation projections on discharge and evapotranspiration is essential to developing robust adaptation strategies. Because P is the key driver influencing hydrological projections, uncertainties in P are more critical than uncertainties in Temp [63]. The results showed MRD between precipitation from the future (RCP8.5) and reference period of about –8% from June to November, but this value varies from –75% (IPSL) to –30%(NORESM1m). Despite that, the GCMs from CMPI5 performed well in the IRB region. However, the models underestimate total rainfall in the dry season compared with observed and reanalysis data, except for HADGEM2-ES [64]. The hydrological projections results experienced a similar pattern as expected. AET and Q decrease mainly in dry months (Figures 9 and 12), supported by previous studies in the Tocantins-Araguaia River basin [65].

5.2. Practical Implications

Different studies in the Amazon suggest that vegetation transpiration during the dry season is sustained at the expense of soil water storage [66–68]. Additionally, the ecological services provided by rainforests depend on the supply of water from the dry months [61]. With the decrease in precipitation predicted by the GCMs, the modeled AET strongly decreased in these months. The modeled streamflow presents the strongest CV at the dry season's end and the rainy season's beginning due to the lack of soil water availability. As previously observed for the IRB, a reduction in soil water storage causes a reduction

in streamflow at the beginning of the wet season (even with average precipitation) [55]. Prolonged droughts previously observed in the Amazon (e.g., 2005 and 2010) have been shown to impact tree mortality (Rowland et al., 2015) and fire occurrence (Chen et al., 2013). A similar effect can be expected in the basin if the predicted scenarios of increased temperature and more extended dry periods are confirmed.

The strong decrease in the reference flow of the dry period Q90 indicates that the flow currently required for a user can be guaranteed for a smaller percentage of the time, and permission for water use should be revised in the future. The increases in the average and maximum flows emphasize the importance of considering the impact of climate change in the design of water storage structures or water drainage to serve the projects and cities in the basin, especially those with a longer useful life.

Climate change affects mining sites in different ways. The increase in air temperature and decrease in precipitation may cause an increase in forest fires, water scarcity, and floods, affecting the viability of mining operations [19]. Transportation routes and mining infrastructure (e.g., infrastructure designed not considering climate changes) will be more susceptible to failure due to the increase in the frequency and severity of floods. These and other risks and opportunities should also be better evaluated, such as a possible reduction in ore moisture and a deterioration in the thermal comfort of outdoor workers.

Understanding the impact of climate change on hydrological processes is essential to managing water resources in watersheds. The Sustainable Development Goals (SDGs) of the United Nations (UN) and several authors [18,26,28,69–73] highlighted this concern. For the mining sector, the International Council on Mining and Metals Report, already quoted, highlights the importance of considering climate change scenarios to manage water use by different users, including mining. This assessment is even more critical in the Amazon Biome, where there are few studies on the topic. Considering the entire basin or influence area in analyzing the climate change risks is important, since obtaining and maintaining a social license to operate will become more difficult in communities in which climate change exacerbates existing vulnerabilities and social conflicts.

6. Conclusions

This paper investigates the impact of future precipitation and temperature projections on discharges and evapotranspiration in the Itacaiúnas River basin using the MGB hydrological model.

The main finds of this study are related to the precipitation, evapotranspiration, and discharges projections. The results indicated that the strengthening of the monsoon seasonal cycle and the lengthening of the dry month period for precipitation and evapotranspiration are expected in the future climate conditions for the IRB. In general, there was an increase in the high flows (from 0 to 20% exceedance probability) and a decrease in the other reference discharges (mainly low flows, with 90% exceedance probability). At mining sites, mainly located in protected areas, climate change may cause an increase in temperature, water scarcity, floods, and a decrease in precipitation.

Finally, the present study can help policymakers identify the need for mitigation policies to address climate change and its effects on the watershed, such as the risk of water shortages and floods for water users due to discharges projections; the impacts on the fauna and flora in riverine habitats due to river flow alterations; the risk of forest fires and impacts to biodiversity due to drier and hotter future climate conditions. Additionally, these results should be used to develop adaptation strategies to ensure the viability of mining operations and safeguard the surrounding environment and communities.

Author Contributions: Conceptualization, P.R.M.P. and R.B.L.C.; Data curation, P.R.M.P. and R.B.L.C.; Formal analysis, P.R.M.P. and R.B.L.C.; Funding acquisition, P.R.M.P.; Investigation, P.R.M.P. and R.B.L.C.; Methodology, P.R.M.P., R.B.L.C., T.C.G., C.P.W.C., R.G.T. and A.M.Q.M.; Project administration, P.R.M.P.; Resources, R.B.L.C. and C.P.W.C.; Software, P.R.M.P.; Supervision, P.R.M.P.; Validation, R.B.L.C.; Visualization, P.R.M.P. and R.B.L.C.; Writing—Original draft, P.R.M.P., R.B.L.C., T.C.G.,

C.P.W.C., R.G.T., A.M.Q.M. and A.C.F.X.; Writing—Review and editing, P.R.M.P. and R.B.L.C. All authors have read and agreed to the published version of the manuscript.

Funding: This paper is a scientific product funding by Vale S.A/Vale Institute of Technology under the code R100603.MC (Project name: “Monitoring of critical events in watersheds where Vale operates”).

Acknowledgments: We thank all reviewers and editors for valuable suggestions. We would like to thank Vale S.A and ITV (Instituto Tecnológico Vale/Vale Institute of Technology). Additionally, thank CNPq for scholarships of Adayana Melo.

Conflicts of Interest: The authors declare that they have no known competing financial interests or personal relationships that could have appeared to influence the work reported in this paper.

References

- Pearce, T.D.; Ford, J.D.; Prno, J.; Duerden, F.; Pittman, J.; Beaumier, M.; Berrang-Ford, L.; Smit, B. Climate change and mining in Canada. *Mitig. Adapt. Strateg. Glob. Chang.* **2011**, *16*, 347–368. [\[CrossRef\]](#)
- Panagoulia, D.; Bárdossy, A.; Lourmas, G. Diagnostic statistics of daily rainfall variability in an evolving climate. *Adv. Geosci.* **2006**, *7*, 349–354. [\[CrossRef\]](#)
- Mota, J.A.; Manesch, M.C.; Souza-Filho, P.W.M.; Torres, V.F.N.; Siqueira, J.O.; Santos, J.F.D.; Matlaba, V. Uma nova proposta de indicadores de sustentabilidade na mineração. *Sustentabilidade Debate* **2017**, *8*, 15–29. [\[CrossRef\]](#)
- Batterham, R. Lessons in Sustainability from the Mining Industry. *Procedia Eng.* **2014**, *83*, 8–15. [\[CrossRef\]](#)
- Čuček, L.; Klemeš, J.; Kravanja, Z. A Review of Footprint analysis tools for monitoring impacts on sustainability. *J. Clean. Prod.* **2012**, *34*, 9–20. [\[CrossRef\]](#)
- Dialga, I. A Sustainability Index of Mining Countries. *J. Clean. Prod.* **2018**, *179*, 278–291. [\[CrossRef\]](#)
- Kunz, N.; Moran, C. Sharing the benefits from water as a new approach to regional water targets for mining companies. *J. Clean. Prod.* **2014**, *84*, 469–474. [\[CrossRef\]](#)
- Northey, S.; Mudd, G.; Saarivuori, E.; Wessman-Jääskeläinen, H.; Haque, N. Water footprinting and mining: Where are the limitations and opportunities? *J. Clean. Prod.* **2016**, *135*, 1098–1116. [\[CrossRef\]](#)
- Brechin, S.R.; Bhandari, M. Perceptions of climate change worldwide. *Wiley Interdiscip. Rev. Clim. Chang.* **2011**, *2*, 871–885. [\[CrossRef\]](#)
- Lobanova, A.; Liersch, S.; Nunes, J.P.; Didovets, I.; Stagl, J.; Huang, S.; Koch, H.; Rivas López, M.D.R.; Maule, C.F.; Hattermann, F.; et al. Hydrological impacts of moderate and high-end climate change across European river basins. *J. Hydrol. Reg. Stud.* **2018**, *18*, 15–30. [\[CrossRef\]](#)
- Mavume, A.F.; Banze, E.; Macie, O.A.; Queface, J. Analysis of Climate Change Projections for Mozambique under the Representative Concentration Pathways. *Atmosphere* **2021**, *12*, 588. [\[CrossRef\]](#)
- Rana, A.; Foster, K.; Bosshard, T.; Olsson, J.; Bengtsson, L. Impact of climate change on rainfall over Mumbai using Distribution-based Scaling of Global Climate Model projections. *J. Hydrol. Reg. Stud.* **2014**, *1*, 107–128. [\[CrossRef\]](#)
- Zheng, H.; Chiew, F.H.S.; Charles, S.; Podger, G. Future climate and runoff projections across South Asia from CMIP5 global climate models and hydrological modelling. *J. Hydrol. Reg. Stud.* **2018**, *18*, 92–109. [\[CrossRef\]](#)
- Siddique, R.; Karmalkar, A.; Sun, F.; Palmer, R. Hydrological extremes across the Commonwealth of Massachusetts in a changing climate. *J. Hydrol. Reg. Stud.* **2020**, *32*, 100733. [\[CrossRef\]](#)
- Chen, Y.; Velicogna, I.; Famiglietti, J.S.; Randerson, J.T. Satellite observations of terrestrial water storage provide early warning information about drought and fire season severity in the Amazon. *J. Geophys. Res. Biogeosci.* **2013**, *118*, 495–504. [\[CrossRef\]](#)
- Rowland, L.; Da Costa, A.C.L.; Galbraith, D.R.; Oliveira, R.S.; Binks, O.J.; Oliveira, A.A.R.; Pullen, A.M.; Doughty, C.E.; Metcalfe, D.B.; Vasconcelos, S.S.; et al. Death from drought in tropical forests is triggered by hydraulics not carbon starvation. *Nature* **2015**, *528*, 119–122. [\[CrossRef\]](#)
- Ndiaye, P.M.; Bodian, A.; Diop, L.; Dezetter, A.; Guilpart, E.; Deme, A.; Ogilvie, A. Future trend and sensitivity analysis of evapotranspiration in the Senegal River Basin. *J. Hydrol. Reg. Stud.* **2021**, *35*, 100820. [\[CrossRef\]](#)
- Greve, P.; Kahil, T.; Mochizuki, J.; Schinko, T.; Satoh, Y.; Burek, P.; Fischer, G.; Tramberend, S.; Burtscher, R.; Langan, S.; et al. Global assessment of water challenges under uncertainty in water scarcity projections. *Nat. Sustain.* **2018**, *1*, 486–494. [\[CrossRef\]](#)
- Odell, S.D.; Bebbington, A.; Frey, K.E. Mining and climate change: A review and framework for analysis. *Extr. Ind. Soc.* **2018**, *5*, 201–214. [\[CrossRef\]](#)
- Schewe, J.; Heinke, J.; Gerten, D.; Haddeland, I.; Arnell, N.W.N.W.; Clark, D.B.D.B.; Dankers, R.; Eisner, S.; Fekete, B.M.; Colón-González, F.J.F.J.; et al. Multimodel assessment of water scarcity under climate change. *Proc. Natl. Acad. Sci. USA* **2013**, *104*, 20167–20172. [\[CrossRef\]](#)
- Woznicki, S.A.; Nejadhashemi, A.P.; Parsinejad, M. Climate change and irrigation demand: Uncertainty and adaptation. *J. Hydrol. Reg. Stud.* **2015**, *3*, 247–264. [\[CrossRef\]](#)
- Bond, R.M.; Stubblefield, A.P.; Van Kirk, R.W. Sensitivity of summer stream temperatures to climate variability and riparian reforestation strategies. *J. Hydrol. Reg. Stud.* **2015**, *4*, 267–279. [\[CrossRef\]](#)

23. Giannini, T.C.; Giuliotti, A.M.; Harley, R.M.; Viana, P.L.; Jaffe, R.; Alves, R.; Pinto, C.E.; Mota, N.F.O.; Caldeira, C.F.; Imperatriz-Fonseca, V.L.; et al. Selecting plant species for practical restoration of degraded lands using a multiple-trait approach. *Austral Ecol.* **2017**, *42*, 510–521. [[CrossRef](#)]
24. Meixner, T.; Manning, A.H.; Stonestrom, D.A.; Allen, D.M.; Ajami, H.; Blasch, K.W.; Brookfield, A.E.; Castro, C.L.; Clark, J.F.; Gochis, D.J.; et al. Implications of projected climate change for groundwater recharge in the western United States. *J. Hydrol.* **2016**, *534*, 124–138. [[CrossRef](#)]
25. Pletterbauer, F.; Melcher, A.; Graf, W. Climate Change Impacts in Riverine Ecosystems. In *Riverine Ecosystem Management*; Aquatic Ecology Series; Schmutz, S., Sendzimir, J., Eds.; Springer: Cham, Switzerland, 2018; Volume 8. [[CrossRef](#)]
26. Brêda, J.P.L.F.; de Paiva, R.C.D.; Collischon, W.; Bravo, J.M.; Siqueira, V.A.; Steinke, E.B. Climate change impacts on South American water balance from a continental-scale hydrological model driven by CMIP5 projections. *Clim. Chang.* **2020**, *159*, 503–522. [[CrossRef](#)]
27. Alves, L.M.; Chadwick, R.; Moise, A.; Brown, J.; Marengo, J.A. Assessment of rainfall variability and future change in Brazil across multiple timescales. *Int. J. Climatol.* **2021**, *41*, E1875–E1888. [[CrossRef](#)]
28. Sorribas, M.V.; Paiva, R.C.D.; Melack, J.M.; Bravo, J.M.; Jones, C.; Carvalho, L.; Beighley, E.; Forsberg, B.; Costa, M.H. Projections of climate change effects on discharge and inundation in the Amazon basin. *Clim. Chang.* **2016**, *136*, 555–570. [[CrossRef](#)]
29. Magrin, G.O.; Marengo, J.; Boulanger, J.P.; Buckeridge, M.S.; Castellano, E.; Poveda, G.; Scarano, F.R.; Vicuña, S.; Alfaro, E.; Anthelme, F.; et al. Central and South America. In *Climate Change 2014: Impacts, Adaptation, and Vulnerability. Part B: Regional Aspects. Contribution of Working Group II to the Fifth Assessment Report of the Intergovernmental Panel on Climate Change*; Field, C.B., Barros, V.R., Dokken, D.J., Mach, K.J., Mastrandrea, M.D., Bilir, T.E., Chatterjee, M., Ebi, K.L., Estrada, Y.O., Genova, R.C., et al., Eds.; Cambridge University Press: Cambridge, UK, 2014; pp. 1499–1566.
30. Barichivich, J.; Gloor, E.; Peylin, P.; Brienen, R.J.W.; Schöngart, J.; Espinoza, J.C.; Pattanayak, K.C. Recent intensification of Amazon flooding extremes driven by strengthened Walker circulation. *Sci. Adv.* **2018**, *4*, eaat8785. [[CrossRef](#)]
31. Butt, M.J.; Umar, M.; Qamar, R. Landslide dam and subsequent dam-break flood estimation using HEC-RAS model in Northern Pakistan. *Nat. Hazards* **2013**, *65*, 241–254. [[CrossRef](#)]
32. Espinoza, J.C.; Ronchail, J.; Marengo, J.A.; Segura, H. Contrasting North–South changes in Amazon wet-day and dry-day frequency and related atmospheric features (1981–2017). *Clim. Dyn.* **2019**, *52*, 5413–5430. [[CrossRef](#)]
33. Leite-Filho, A.T.; Costa, M.H.; Fu, R. The southern Amazon rainy season: The role of deforestation and its interactions with large-scale mechanisms. *Int. J. Climatol.* **2020**, *40*, 2328–2341. [[CrossRef](#)]
34. Marengo, J.A.; Chou, S.C.; Kay, G.; Alves, L.M.; Pesquero, J.F.; Soares, W.R.; Santos, D.C.; Lyra, A.A.; Sueiro, G.; Betts, R.; et al. Development of regional future climate change scenarios in South America using the Eta CPTEC/HadCM3 climate change projections: Climatology and regional analyses for the Amazon, São Francisco and the Paraná River basins. *Clim. Dyn.* **2012**, *38*, 1829–1848. [[CrossRef](#)]
35. Ronchail, J.; Espinoza, J.C.; Drapeau, G.; Sabot, M.; Cochonneau, G.; Schor, T. The flood recession period in Western Amazonia and its variability during the 1985–2015 period. *J. Hydrol. Reg. Stud.* **2018**, *15*, 16–30. [[CrossRef](#)]
36. Tomasella, J.; Borma, L.S.; Marengo, J.A.; Rodriguez, D.A.; Cuartas, L.A.; Nobre, C.A.; Prado, M.C.R. The droughts of 1996–1997 and 2004–2005 in Amazonia: Hydrological response in the river main-stem. *Hydrol. Processes* **2011**, *25*, 1228–1242. [[CrossRef](#)]
37. De Amorim, P.B.; Chaffe, P.L.B. Integrating climate models into hydrological modelling: What’s going on in Brazil? *Rev. Bras. Recur. Hídric.* **2019**, *24*, e31. [[CrossRef](#)]
38. OECD. *Regulatory Governance in the Mining Sector in Brazil*; OECD Publishing: Paris, France, 2022. [[CrossRef](#)]
39. Pontes, P.R.M.; Cavalcante, R.B.L.; Sahoo, P.K.; Silva Júnior, R.O.D.; da Silva, M.S.; Dall’Agnol, R.; Siqueira, J.O. The role of protected and deforested areas in the hydrological processes of Itacaiúnas River Basin, eastern Amazonia. *J. Environ. Manag.* **2019**, *235*, 488–499. [[CrossRef](#)]
40. Souza-Filho, P.W.M.; Nascimento, W.R.; Santos, D.C.; Weber, E.J.; Silva, R.O.; Siqueira, J.O. A GEOBIA approach for multitemporal land-cover and land-use change analysis in a tropical watershed in the southeastern Amazon. *Remote Sens.* **2018**, *10*, 1683. [[CrossRef](#)]
41. Alvares, C.A.; Stape, J.L.; Sentelhas, P.C.; De Moraes Gonçalves, J.L.; Sparovek, G. Köppen’s climate classification map for Brazil. *Meteorol. Z.* **2013**, *22*, 711–728. [[CrossRef](#)]
42. Cavalcante, R.B.L.; Pontes, P.R.M.; Souza-Filho, P.W.M.; de Souza, E.B. Opposite Effects of Climate and Land Use Changes on the Annual Water Balance in the Amazon Arc of Deforestation. *Water Resour. Res.* **2019**, *55*, 3092–3106. [[CrossRef](#)]
43. Taylor, K.E.; Stouffer, R.J.; Meehl, G.A. An overview of CMIP5 and the experiment design. *Bull. Am. Meteorol. Soc.* **2012**, *93*, 485–498. [[CrossRef](#)]
44. Hempel, S.; Frieler, K.; Warszawski, L.; Schewe, J.; Piontek, F. A trend-preserving bias correction—The ISI-MIP approach. *Earth Syst. Dynam.* **2013**, *4*, 219–236. [[CrossRef](#)]
45. Collischonn, W.; Allasia, D.; Da Silva, B.C.; Tucci, C.E.M. The MGB-IPH model for large-scale rainfall—Runoff modelling. *Hydrol. Sci. J.* **2007**, *52*, 878–895. [[CrossRef](#)]
46. Pontes, P.R.M.; Fan, F.M.; Fleischmann, A.S.; de Paiva, R.C.D.; Buarque, D.C.; Siqueira, V.A.; Jardim, P.F.; Sorribas, M.V.; Collischonn, W. MGB-IPH model for hydrological and hydraulic simulation of large floodplain river systems coupled with open source GIS. *Environ. Model. Softw.* **2017**, *94*, 1–20. [[CrossRef](#)]

47. Siqueira, V.; Paiva, R.; Fleischmann, A.; Fan, F.; Ruhoff, A.; Pontes, P.; Paris, A.; Calmant, S.; Collischonn, W. Toward continental hydrologic–hydrodynamic modeling in South America. *Hydrol. Earth Syst. Sci. Discuss.* **2018**, *22*, 4815–4842. [[CrossRef](#)]
48. Fleischmann, A.; Siqueira, V.; Paris, A.; Collischonn, W.; Paiva, R.; Pontes, P.; Crétaux, J.-F.; Bergé-Nguyen, M.; Biancamaria, S.; Gosset, M.; et al. Modelling hydrologic and hydrodynamic processes in basins with large semi-arid wetlands. *J. Hydrol.* **2018**, *561*, 943–959. [[CrossRef](#)]
49. Wigmosta, M.S.; Vail, L.W.; Lettenmaier, D.P. A distributed hydrology–vegetation model for complex terrain. *Water Resour. Res.* **1994**, *30*, 1665–1679. [[CrossRef](#)]
50. Todini, E. The ARNO rainfall-runoff model. *J. Hydrol.* **1996**, *175*, 339–382. [[CrossRef](#)]
51. Takaku, J.; Tadono, T.; Tsutsui, K.; Ichikawa, M. Validation of “Aw3D” Global Dsm Generated from Alos Prism. ISPRS Annals of Photogrammetry, Remote Sensing and Spatial Information Sciences. In Proceedings of the XXIII ISPRS Congress, Prague, Czech Republic, 12–19 July 2016; Volume III–4, pp. 25–31. [[CrossRef](#)]
52. O’Loughlin, F.E.; Paiva, R.C.D.; Durand, M.; Alsdorf, D.E.; Bates, P.D. A multi-sensor approach towards a global vegetation corrected SRTM DEM product. *Remote Sens. Environ.* **2016**, *182*, 49–59. [[CrossRef](#)]
53. Nobre, A.D.; Cuartas, L.A.; Hodnett, M.; Rennó, C.D.; Rodrigues, G.; Silveira, A.; Waterloo, M.; Saleska, S. Height Above the Nearest Drainage—A hydrologically relevant new terrain model. *J. Hydrol.* **2011**, *404*, 13–29. [[CrossRef](#)]
54. Yamazaki, D.; De Almeida, G.A.M.; Bates, P.D. Improving computational efficiency in global river models by implementing the local inertial flow equation and a vector-based river network map. *Water Resour. Res.* **2013**, *49*, 7221–7235. [[CrossRef](#)]
55. Cavalcante, R.B.L.; Pontes, P.R.M.; Tedeschi, R.G.; Costa, C.P.W.; Ferreira, D.B.S.; Souza-Filho, P.W.M.; de Souza, E.B. Terrestrial water storage and Pacific SST affect the monthly water balance of Itacaiúnas River Basin (Eastern Amazonia). *Int. J. Climatol.* **2020**, *40*, 3021–3035. [[CrossRef](#)]
56. Collischonn, B.; Collischonn, W. Rainfall as proxy for evapotranspiration predictions. *Proc. Int. Assoc. Hydrol. Sci.* **2016**, *374*, 35–40. [[CrossRef](#)]
57. Escobar, H. Deforestation in the Brazilian Amazon is still rising sharply. *Science* **2020**, *369*, 613. [[CrossRef](#)]
58. Giannini Costa, W.F.; Borges, R.C.; Miranda, L.; da Costa, C.P.W.; Saraiva, A.M.; Imperatriz Fonseca, V.L. Climate change in the Eastern Amazon: Crop-pollinator and occurrence-restricted bees are potentially more affected. *Reg. Environ. Chang.* **2020**, *20*, 9. [[CrossRef](#)]
59. Jaffé, R.; Veiga, J.C.; Pope, N.S.; Lanes, É.C.M.; Carvalho, C.S.; Alves, R.; Andrade, S.C.S.; Arias, M.C.; Bonatti, V.; Carvalho, A.T.; et al. Landscape genomics to the rescue of a tropical bee threatened by habitat loss and climate change. *Evol. Appl.* **2019**, *12*, 1164–1177. [[CrossRef](#)]
60. Miranda, L.S.; Imperatriz-Fonseca, V.L.; Giannini, T.C. Climate change impact on ecosystem functions provided by birds in southeastern Amazonia. *PLoS ONE* **2019**, *14*, e215229. [[CrossRef](#)]
61. Boisier, J.P.; Ciais, P.; Ducharne, A.; Guimberteau, M. Projected strengthening of Amazonian dry season by constrained climate model simulations. *Nat. Clim. Chang.* **2015**, *5*, 656–660. [[CrossRef](#)]
62. Llopart, M.; Simões Reboita, M.; Porfirio da Rocha, R. Assessment of multi-model climate projections of water resources over South America CORDEX domain. *Clim. Dyn.* **2020**, *54*, 99–116. [[CrossRef](#)]
63. Her, Y.; Yoo, S.H.; Cho, J.; Hwang, S.; Jeong, J.; Seong, C. Uncertainty in hydrological analysis of climate change: Multi-parameter vs. multi-GCM ensemble predictions. *Sci. Rep.* **2019**, *9*, 4974. [[CrossRef](#)]
64. Yin, L.; Fu, R.; Shevliakova, E.; Dickinson, R.E. How well can CMIP5 simulate precipitation and its controlling processes over tropical South America? *Clim. Dyn.* **2013**, *41*, 3127–3143. [[CrossRef](#)]
65. Ho, J.T.; Thompson, J.R.; Brierley, C. Projections of hydrology in the Tocantins-Araguaia Basin, Brazil: Uncertainty assessment using the CMIP5 ensemble. *Hydrol. Sci. J.* **2016**, *61*, 551–567. [[CrossRef](#)]
66. Belk, E.L.; Markewitz, D.; Rasmussen, T.C.; Carvalho, E.J.M.; Nepstad, D.C.; Davidson, E.A. Modeling the effects of throughfall reduction on soil water content in a Brazilian Oxisol under a moist tropical forest. *Water Resour. Res.* **2007**, *43*, W08432. [[CrossRef](#)]
67. Christoffersen, B.O.; Restrepo-Coupe, N.; Arain, M.A.; Baker, I.T.; Cestaro, B.P.; Ciais, P.; Fisher, J.B.; Galbraith, D.; Guan, X.; Gulden, L.; et al. Mechanisms of water supply and vegetation demand govern the seasonality and magnitude of evapotranspiration in Amazonia and Cerrado. *Agric. For. Meteorol.* **2014**, *191*, 33–50. [[CrossRef](#)]
68. Negrón Juárez, R.I.; Hodnett, M.G.; Fu, R.; Gouden, M.L.; von Randow, C. Control of dry season evapotranspiration over the Amazonian forest as inferred from observation at a Southern Amazon forest site. *J. Clim.* **2007**, *20*, 2827–2839. [[CrossRef](#)]
69. Gao, C.; Liu, L.; Ma, D.; He, K.; Xu, Y.P. Assessing responses of hydrological processes to climate change over the southeastern Tibetan Plateau based on resampling of future climate scenarios. *Sci. Total Environ.* **2019**, *664*, 737–752. [[CrossRef](#)]
70. Gesualdo, G.C.; Oliveira, P.T.; Rodrigues, D.B.B.; Gupta, H.V. Assessing water security in the São Paulo metropolitan region under projected climate change. *Hydrol. Earth Syst. Sci.* **2019**, *23*, 4955–4968. [[CrossRef](#)]
71. Hoang, L.P.; van Vliet, M.T.H.; Kumm, M.; Lauri, H.; Koponen, J.; Supit, I.; Leemans, R.; Kabat, P.; Ludwig, F. The Mekong’s future flows under multiple drivers: How climate change, hydropower developments and irrigation expansions drive hydrological changes. *Sci. Total Environ.* **2019**, *649*, 601–609. [[CrossRef](#)]
72. Wada, Y.; Bierkens, M.F.P. Sustainability of global water use: Past reconstruction and future projections. *Environ. Res. Lett.* **2014**, *9*, 104003. [[CrossRef](#)]
73. Xu, R.; Hu, H.; Tian, F.; Li, C.; Khan, M.Y.A. Projected climate change impacts on future streamflow of the Yarlung Tsangpo-Brahmaputra River. *Glob. Planet. Chang.* **2019**, *175*, 144–159. [[CrossRef](#)]